JOURNAL OF CATALYSIS 66, 36–48 (1980)

Kinetics, Limit Cycles, and Mechanism of the Ethylene Oxidation on Platinum

C. G. VAYENAS, B. LEE, AND J. MICHAELS

Massachusetts Institute of Technology, Cambridge, Massachusetts 02139

Received November 26, 1979; revised May 12, 1980

The oxidation of ethylene on polycrystalline Pt films was studied in a CSTR at atmospheric pressure and temperatures between 200 and 400°C. The new technique of solid electrolyte potentiometry (SEP) was used to monitor the activity of oxygen on the metal catalyst. To this end the platinum film catalyst also served as one of the electrodes of a solid-electrolyte oxygen concentration cell and the open-circuit emf of the cell was monitored during reaction. It was found that the steady-state surface oxygen activity a_0 satisfies the equation $a_0 = K_s P_{O_2}/P_{ET}$, where K_s depends on temperature only. The reaction rate is first order in ethylene and adsorbed oxygen. Over a certain range of temperature and gas-phase composition both the surface oxygen activity and the reaction rate exhibit self-sustained oscillations. Limit cycles appear only over a well-defined range of surface oxygen activity a_0 values. The oscillations can be explained in terms of the stability of a surface platinum oxide. The reaction mechanism is discussed in light of these observations.

INTRODUCTION

The catalytic oxidation of hydrocarbons on Pt has received wide attention in recent years due to the use of platinum as one of the active components in automotive exhaust catalytic converters. Work in this area prior to 1970 has been summarized in several reviews (*1–3*).

The kinetics of the ethylene oxidation on silica-supported Pt have been studied in some detail by Cant and Hall (*4*). They observed a negative-order rate dependence on ethylene and almost first-order dependence on oxygen. Carberry (*5*) has studied the effect of the average dimension of the crystallites of Pt/Al_2O_3 catalysts on the specific rate of ethylene oxidation. He found that the specific rate increases with increasing crystallite size and proposed the following rate expression in excess air:

$$R = \frac{c_1 P_{ET}}{1 + (c_1/c_2) P_{ET}^2},$$

where c_1 and c_2 are increasing functions of temperature. He suggested an Eley–Rideal-type mechanism with the rate controlled by oxygen adsorption in excess ethylene and by the reaction between adsorbed oxygen and gaseous ethylene in excess air.

The use of the new technique of solid-electrolyte potentiometry (SEP) permits an *in situ* measurement of the thermodynamic activity of oxygen adsorbed on metal film catalysts. To this end the metal catalyst also serves as one of the electrodes of a solid-electrolyte oxygen concentration cell. The other electrode is exposed to a reference gas. The oxygen activity of the catalyst can then be obtained by measuring the open-circuit emf of the cell. Originally proposed by Wagner (*6*), this simple technique has been used already in conjunction with kinetic measurements to study the oxidation of SO_2 on several metals including Pt (*7, 8*). The purpose of the present work was to examine the mechanism of the ethylene oxidation on Pt and compare the surface oxygen activity measurements with similar measurements on Ag (*9*).

EXPERIMENTAL METHODS

Catalyst and Apparatus

The kinetic studies were carried out in the flow reactor shown in Fig. 1. The reactor has been shown to be well mixed

0021-9517/80/110036-13$02.00/0

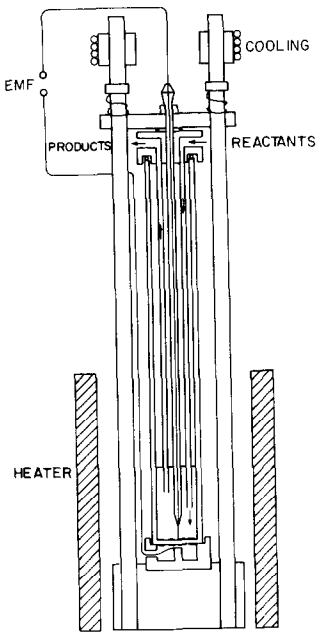

FIG. 1. Reactor-cell configuration.

(CSTR) over the range of flow rates employed in the present study by using an ir CO_2 analyzer to obtain its residence time distribution (*9, 22*). A schematic diagram of the apparatus is shown in Fig. 2. The volume of the reactor was 30 cm^3. The Pt catalyst film was deposited on the flat bottom of a stabilized zirconia tube (8% yttria-stabilized zirconia) using Englehard 05-X

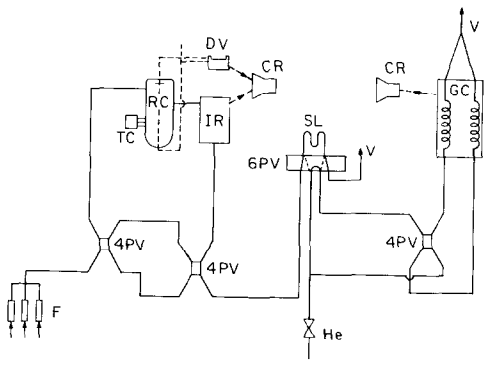

FIG. 2. Schematic diagram of the apparatus: (F) Flow meters; (4PV) four-port valve; (6PV) six-port valve; (RC) reactor cell; (TC) temperature controller; (IR) Infrared CO_2 analyzer; (DV) differential voltmeter; (SL) sampling loop; (GC) gas chromatograph; (CR) strip-chart recorder; (V) vent.

platinum paste (reactor 1) or Englehard A-3788 paste (reactor 2) and drying and calcining in air at 600°C for 5 h. The Pt film, approximately 5 μm thick, was examined with XPS (Fig. 3). The superficial surface area of the film was 2 cm^2. The true surface area, too low to be measured accurately by BET, was estimated as follows. Oxygen was allowed to chemisorb on the Pt film and the reactor was subsequently purged with high-purity N_2 for a time t at least eight times longer than the residence time τ of the CSTR ($\tau \sim 5$ s). Then the reactor was purged with ethylene and the total amount of CO_2 formed was determined by an ir CO_2 analyzer (Beckman Model 864) continuously monitoring the CSTR output. By varying τ one can study the kinetics of oxygen desorption from platinum (which are much slower than the ethylene–oxygen reaction kinetics). By extrapolating to $t = 0$ one can determine the maximum number N_{max} of oxygen moles adsorbed on the catalyst. N_{max} is thus estimated to be $(8 \pm 2) \times 10^{-7}$ mol O_2 for reactor 2, in which the steady-state kinetics and limit cycles were studied in detail.

A similar Pt film was deposited on the outside wall of the stabilized zirconia tube. This Pt film was exposed to air and served as the reference electrode.

An appropriately machined stainless-steel cap was clamped to the open end of the tube. The cap had provision for introduction of reactants, removal of products, as well as for introduction of a Pt wire, partly enclosed in a Pyrex tube to make contact with the internal Pt film catalyst electrode. The open-circuit emf of the oxygen concentration cell was measured with a solid-state differential voltmeter (J. Fluke Model 891 A) with an input impedance of 10^8 ohms and infinite resistance at null. The reactor temperature was controlled within 2°C and also measured with a second thermocouple touching the wall of the stabilized zirconia tube 1 mm from the outside electrode. In some of the experiments a third thermocouple was directly attached to

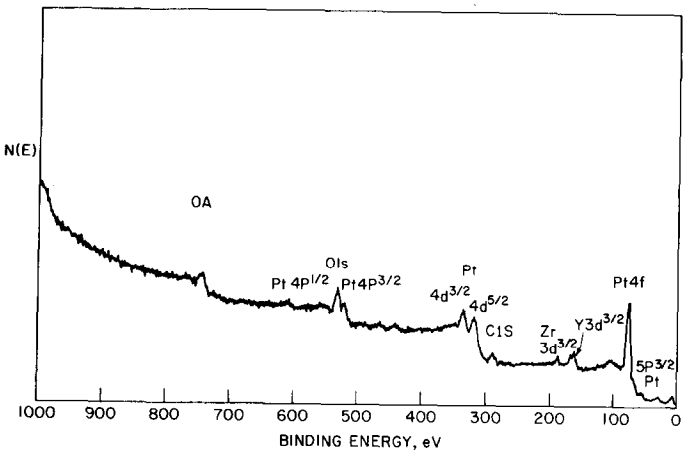

FIG. 3. XPS survey spectrum of the Pt catalyst-electrode supported on the ZrO_2–Y_2O_3 electrolyte (Mg$K\alpha$ source).

the metal catalyst film. At steady state the readings of all three thermocouples agreed within 2°C.

The reactants were Matheson certified C_2H_4 diluted in N_2 and Matheson zero gas air. They could be further diluted with N_2. Calibrated rotameters were used to measure the total flow rate.

Reactants and products were analyzed for ethylene, CO_2, O_2, and N_2 using a Perkin–Elmer Model 3920 B gas chromatograph with a TC detector. A Porapak Q column was used to separate air, CO_2, and ethylene and a molecular sieve 5A column separated N_2 and O_2.

The concentration of CO_2 in the products was also directly monitored by means of an ir CO_2 analyzer (Beckman Model 864) with a response time of 0.5 s. This turned out to be essential for the study of the observed rate oscillations. At steady state the concentration of CO_2 as measured by the ir analyzer was in very good agreement (within 2%) with the GC measurement.

Measurement of the Oxygen Activity

The simple new technique of solid electrolyte potentiometry (SEP), previously employed to study the SO_2 oxidation on noble metals (*8*), was used to measure *in situ* the thermodynamic activity of oxygen on the Pt catalyst. The open-circuit emf of the solid-electrolyte cell utilized here is

$$E = (\tfrac{1}{4}F)(\mu_{O_2(Pt)cat.} - \mu_{O_2(Pt)ref.}), \quad (1)$$

where F is the Faraday constant and $\mu_{O_2(Pt)}$ is the chemical potential of oxygen adsorbed on the Pt electrodes. This is derived on the assumption that the stabilized zirconia solid electrolyte is a purely anionic (O^{2-}) conductor and that the dominant exchange current reaction involves O^{2-} and adsorbed oxygen. Equation (1) includes a limiting case the usual Nernst equation

$$E = \frac{RT}{4F} \ln \frac{P'_{O_2}}{P_{O_2}} \quad (2)$$

which is valid only when no chemical reaction involving the gas phase proceeds at the electrode surface (*10*). In the general case it is the activity of oxygen adsorbed on the electrodes rather than the gas-phase oxygen activity which determines the open-circuit emf (*11*).

The chemical potential of oxygen at the reference electrode which is in contact with air (P_{O_2} = 0.21 bar) is given by

$$\mu_{O_2(Pt)ref.} = \mu^{\circ}_{O_2(g)} + RT \ln (0.21), \quad (3)$$

where $\mu^{\circ}_{O_2(g)}$ is the standard chemical potential of oxygen at the temperature of interest. Since at temperatures of catalytic inter-

est oxygen is well known to chemisorb dissociatively on platinum (*12*), one can define the activity of oxygen atoms on the catalyst a_0 by a similar equation:

$$\mu_{O_2(cat)} = \mu^{\circ}_{O_2(g)} + RT \ln a_0^2. \quad (4)$$

Therefore a_0^2 expresses the partial pressure of gaseous oxygen that would be in thermodynamic equilibrium with oxygen atoms adsorbed on the platinum surface, if such an equilibrium were established.

Combining (1), (3), and (4), a_0 (bar$^{1/2}$) is given by

$$a_0 = (0.21)^{1/2} \exp \frac{2FE}{RT}. \quad (5)$$

If equilibrium is established between gaseous oxygen in the reactor and oxygen on the catalyst, then

$$a_0^2 = P_{O_2}.$$

On the other hand, if the intrinsic rate of reaction of chemisorbed oxygen is comparable to or greater than the intrinsic rate of oxygen adsorption, then, in general, $a_0^2 < P_{O_2}$.

RESULTS

The Surface Oxygen Activity during Reaction

The correct performance of the solid-electrolyte cell was verified by introducing into the reactor various air–N_2 mixtures of known oxygen partial pressure and measuring open-circuit voltages in agreement with the Nernst equation

$$E = \frac{RT}{4F} \ln \frac{P_{O_2}}{0.21}$$

within 2 mV.

Below 250°C very long times were necessary for establishment of steady-state emf measurements and no data were taken in this region.

Introduction of ethylene–air mixtures in the previously air-equilibrated reactor resulted in open-circuit emf of the order of −150 mV, indicating that the surface oxygen activity a_0 given by (5) is of the order of 10^{-3} atm$^{1/2}$ and that $a_0^2 < P_{O_2}$. Therefore under reaction conditions the surface oxygen is not in thermodynamic equilibrium with gas-phase oxygen.

It was observed that a_0 decreases with increasing P_{ET} and increases with increasing P_{O_2}. No dependence of a_0 on P_{CO_2} or P_{H_2O} was observed. Statistical analysis of the results showed that the data could be correlated rather accurately by the expression

$$\frac{P_{ET} \cdot a_0}{P_{O_2}} = K_s, \quad (6)$$

where K_s is a function of temperature only. This is shown in Fig. 4. Equation (6) was valid over the entire range of temperatures investigated (260 < T < 400°C) and over a very wide range of gas-phase compositions (P_{ET}/P_{O_2} in the CSTR varying between 10 and 10^{-2}).

For values of P_{ET}/P_{O_2} above approximately 0.3, the open-circuit emf, and therefore a_0, exhibits oscillatory behavior, although the average a_0 value during these oscillations is still in reasonable agreement with Eq. (6). This is discussed below in

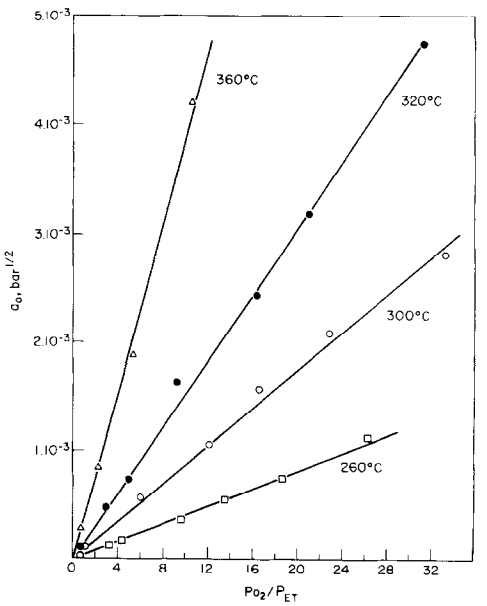

FIG. 4. Surface oxygen activity dependence on gas-phase composition.

conjunction with the observed rate oscillations.

The temperature dependence of K_s is exhibited in Fig. 5 for reactors 1 and 2. Although the slope of ln K_s vs $1/T$ was found to be practically the same for all different Pt pastes and calcination procedures used, the preexponential factor was found to differ by as much as a factor of 3. This may be due to the effect of crystallite size on the kinetics (*5*).

Kinetic Measurements

The kinetics were studied at temperatures between 200 and 400°C, ethylene partial pressures up to 0.02 bar, and oxygen partial pressures up to 0.2 bar. Under these conditions no detectable conversion to partially oxygenated products was observed. The zirconia tube itself, before deposition of the Pt electrode, was totally inactive for ethylene oxidation even at 450°C.

The inlet stream impinged directly on the catalyst film with velocities of the order of 1–2 m/s to avoid mass transfer limitations. The surface oxygen activity a_0 was uniquely determined by P_{ET}/P_{O_2} and temperature and did not depend on the flow rate varying between 100 and 600 cm^3 (STP)/min. This shows that the measured low values of a_0 are not due to diffusional limitations.

Diffusional effects inside the porous Pt film are also negligible because of the very small film thickness ($L \approx 5$ μm). If the internal diffusional resistance were significant, then a_0, which is measured at the gas–electrode–electrolyte interline, would decrease with increasing T at constant gas composition, contrary to what was observed (Eq. (6) and Fig. 5). The absence of internal diffusional effects can also be illustrated by an estimation of the catalyst Thiele modulus $\Phi = L(K/D_e)^{1/2}$. Assuming a catalyst porosity of 0.5 and tortuosity of 2, Φ can be shown to be less than 0.3 at all conditions studied. This has also been shown experimentally by varying the thickness of similar porous Pt and Ag films used to study SO_2 and ethylene oxidation, respectively, at similar global oxidation rates; no change in a_0 with film thickness was observed at constant gas composition (*8, 23*).

Over the temperature range investigated the rate is first order in ethylene and zero order in oxygen for low values of ethylene

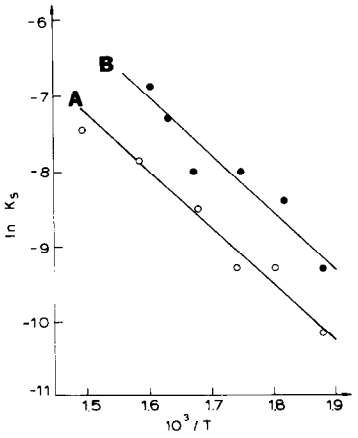

FIG. 5. Temperature dependence of K_s for catalysts A (reactor 1) and B (reactor 2).

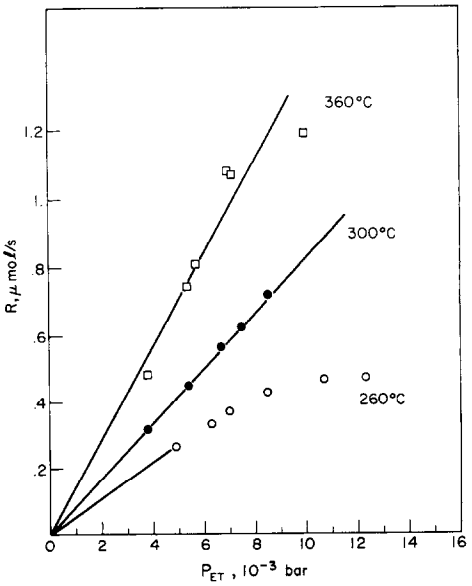

FIG. 6. Rate dependence on P_{ET} for high P_{O_2} (>5 × 10^{-2} bar).

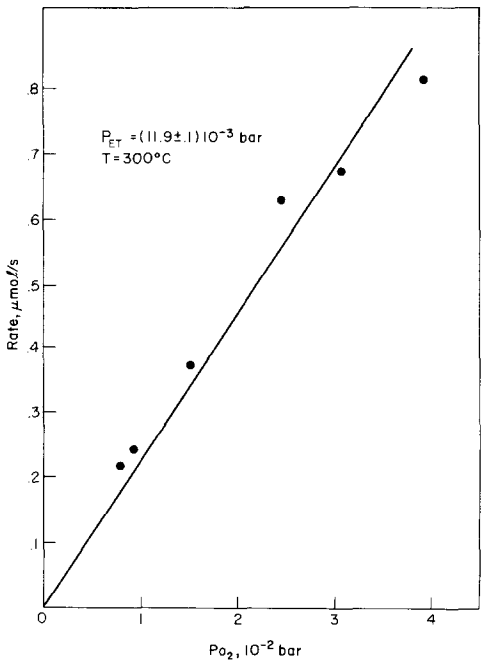

FIG. 7. Rate dependence on P_{O_2} for high P_{ET}.

partial pressure (Fig. 6). In this region (I) the apparent activation energy is fairly low, of the order of 25 kJ/mol. At higher values of P_{ET} the rate becomes first order in oxygen and almost zero order in ethylene (Fig. 7) with an apparent activation energy of 70 kJ/mol. No negative-order dependence of the rate on ethylene was observed. However, in this region (II) the accuracy of the data is severely reduced due to the observed rate oscillations. Several rate expressions were tried in order to describe the kinetic behavior in both regions. The most successful one was

$$r = \frac{K_1K_2P_{ET}P_{O_2}}{K_1P_{O_2} + K_2P_{ET}} = K_2P_{ET}\frac{1}{1 + K_2P_{ET}/K_1P_{O_2}} \quad (7)$$

with $K_1 = 145 \exp(-70{,}000/RT)$ mol/s, $K_2 = 5.8 \times 10^{-3} \exp(-21{,}000/RT)$ mol/s, $R = 8.31$ J/mol · K. Figure 8 shows that the rate is first order in ethylene at constant $N_3'(P_{ET}/P_{O_2})$.

This rate expression accounts also for the observed break in the Arrhenius plot at constant P_{ET} and P_{O_2} (Fig. 9).

Rate and Surface Oxygen Activity Oscillations

At temperatures between 240 and 360°C and fuel-rich ethylene–air mixtures it was observed that the rate of CO_2 production as well as the surface oxygen activity exhibits self-sustained oscillations. There exist conditions under which the oscillations are quite regular, almost sinusoidal (Fig. 10), but also conditions under which both rate and surface oxygen activity exhibit "spikes" above an average value.

The period and amplitude of the oscillations are strongly dependent on temperature, residence time, and inlet ethylene to oxygen ratio. Oscillations occur only with ethylene/oxygen ratios above $\frac{1}{3}$. One common feature of the oscillations is that surface oxygen activity and rate of CO_2 production oscillate simultaneously with decreasing surface oxygen activity always corresponding to increasing rate. Typical "periods" are between 5 and 360 s and typical amplitudes are 5–10 mV for the emf

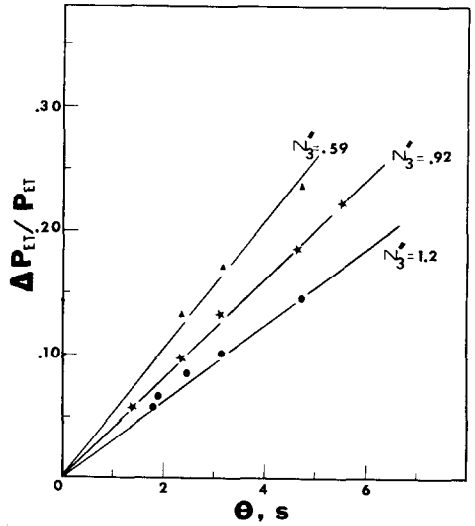

FIG. 8. Ratio of ($P_{ET,feed} - P_{ET}$) to P_{ET} vs residence time at constant N_3' ($\equiv P_{ET}/P_{O_2}$). Temperature = 300°C.

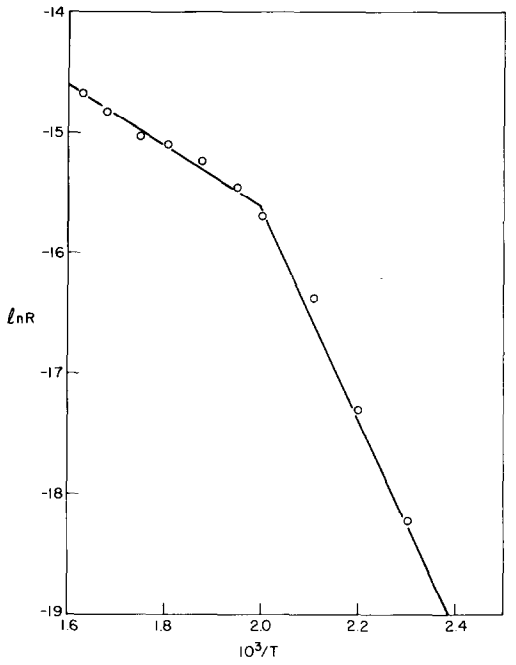

FIG. 9. Rate vs temperature at constant composition $P_{ET} = (1.4 \pm 0.1) \times 10^{-2}$ bar, $P_{O_2} = (1.2 \pm 0.2) \times 10^{-2}$ bar. Transition from range I (high T) to range II (low T).

and up to 2×10^{-3} bar for the partial pressure of CO_2 in the products.

The effect of temperature at constant residence time and inlet composition is demonstrated in Fig. 11. Below 240°C the rate does not oscillate. At 240°C the rate exhibits limit-cycle behavior with a period of 36 s. As the temperature is increased further the amplitude increases and goes through a maximum at 280°C while the frequency increases continuously, until at 360°C the oscillations disappear. The upper and lower temperature limits for rate oscillations (240 and 360°C, respectively) were found to be only slightly sensitive to changes in residence time and gas-phase composition.

The effect of the inlet ethylene to oxygen ratio N_3 on the frequency of the limit cycles is shown in Figs. 12 and 13. For $N_3 < 0.33$ no limit cycles are observed. A stable steady state is obtained instead. For larger N_3 the frequency is a linear function of N_3 at constant temperature and residence time.

The effect of residence time Θ at constant temperature and ethylene to oxygen ratio N_3 is shown in Fig. 14. The frequency of the limit cycles is proportional to the residence time.

A very interesting feature of the oscillations is that, at constant temperature, they take place only when the surface oxygen activity a_0 is above a critical value $a_0^*(T)$ characteristic of T and below a second critical value $a_{0,s}$ roughly equal to 3 K_s, corresponding to the stoichiometric oxygen/ethylene ratio. This is demonstrated in Figs. 15 and 16 where the period and frequency of the limit cycles are plotted vs the average value of a_0 during the limit cycle. For $a_0 = a_0^*$ the frequency becomes infinite and the amplitude approaches zero.

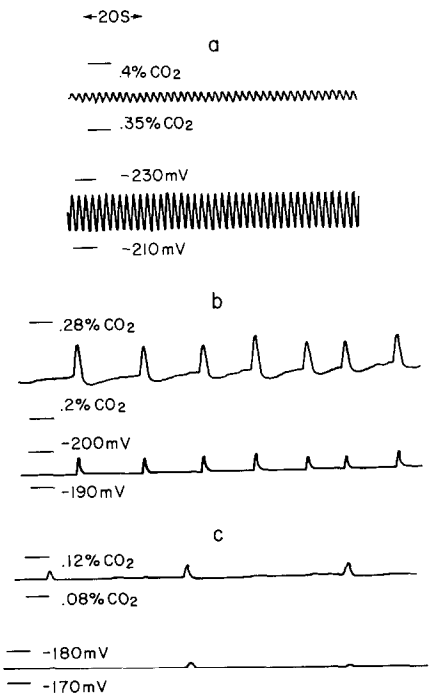

FIG. 10. Rate and surface oxygen activity oscillations at 300°C. (a) $P_{ET} = 15 \times 10^{-3}$ bar, $P_{O_2} = 5 \times 10^{-3}$ bar, residence time $t = 5$ s; (b) $P_{ET} = 9 \times 10^{-3}$ bar, $P_{O_2} = 11 \times 10^{-3}$ bar, $t = 4$ s; (c) $P_{ET} = 4.5 \times 10^{-3}$ bar, $P_{O_2} = 13 \times 10^{-3}$ bar, $t = 2$ s.

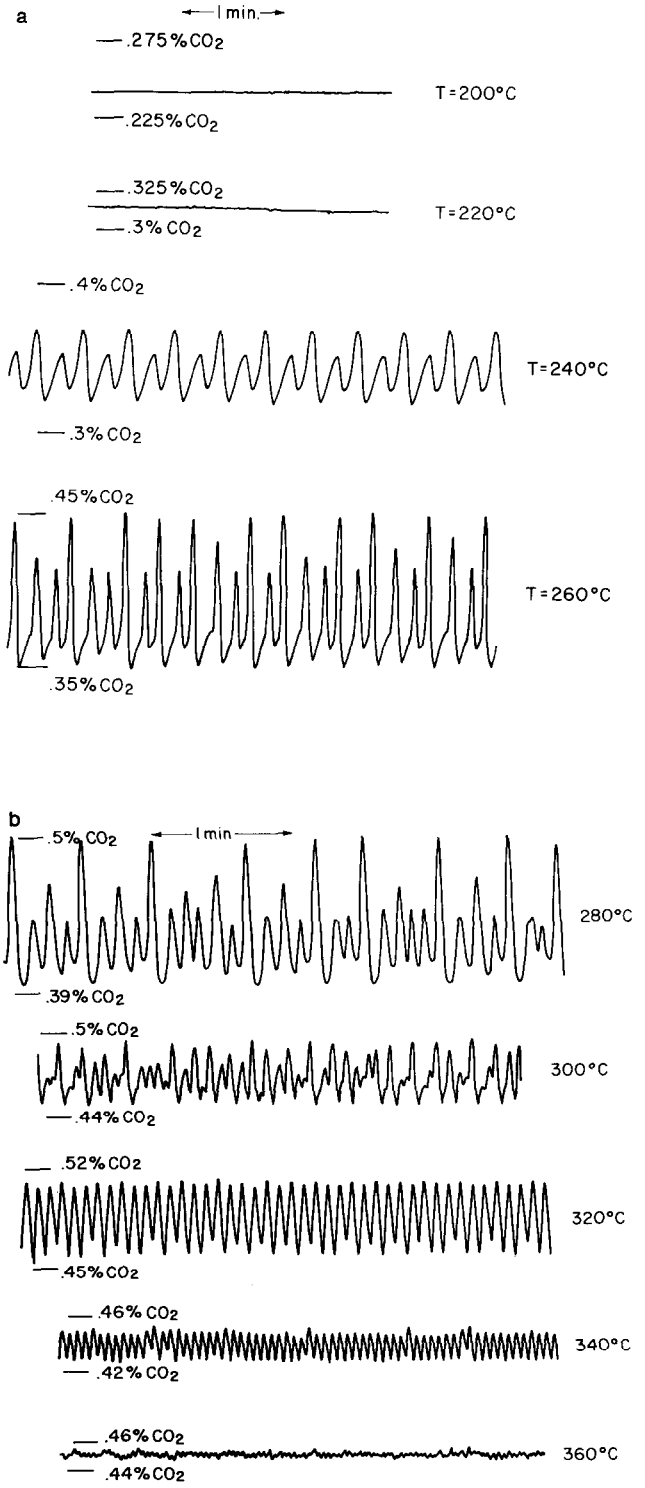

FIG. 11. (a, b) Effect of temperature at constant feed composition ($P_{ET} = 16.5 \times 10^{-3}$ bar, $P_{O_2} = 2 \times 10^{-2}$ bar) and flow rate (200 cm³ (STP)/min).

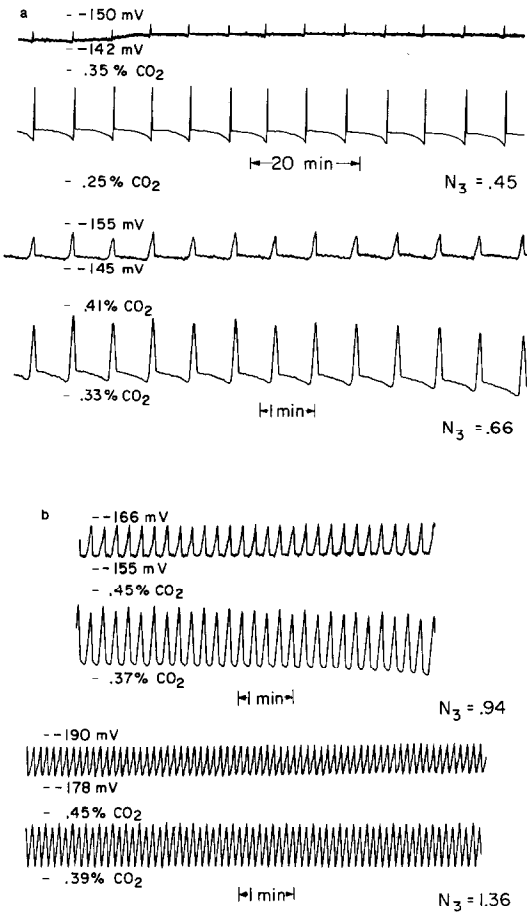

FIG. 12. (a, b) Effect of increasing N_3 at constant T (300°C) and residence time (4.7 s).

For $a_0 \sim a_{0,s}$ the period becomes infinite, i.e., a stable steady state is observed.

The oscillations are isothermal within 0.5°C as was determined by attaching a thermocouple directly to the catalyst film and observing no temperature oscillations and less than 2°C difference between the catalyst film temperature and the ambient gas temperature. This is reasonable in view of the fact that the maximum turnover numbers (molecules/sec-site) in the present study are of the order of 0.4 on the basis of the surface area estimation. These compare well with those of other investigators who studied similar oscillations of the CO oxidation rate on Pt in gradientless reactors (*17*).

DISCUSSION

Steady-State Kinetics

The observed steady-state kinetic behavior is in reasonable agreement with previous investigations (*4, 5*), especially taking into account the different temperature range employed in the present study. Detailed kinetic measurements were not extended below 250°C. At such low temperatures it becomes practically impossible to use SEP for the oxygen activity measurement due to the very high resistivity of the stabilized zirconia electrolyte.

However, it is clear from the rate expression and the temperature dependence of K_1 and K_2 that at low temperatures the rate is

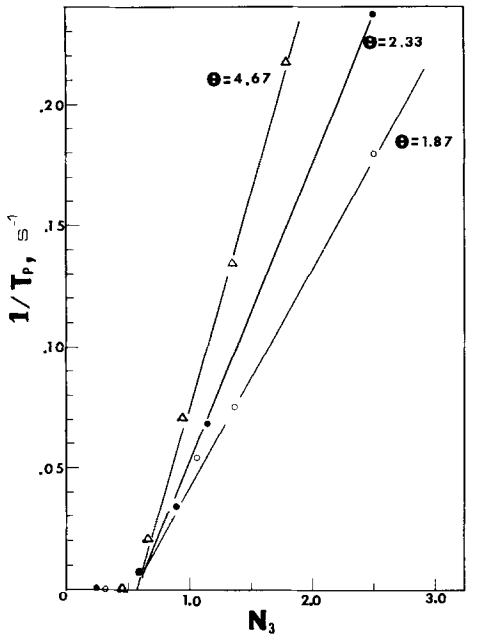

FIG. 13. Limit-cycle frequency vs N_3 at T = 300°C.

first order in oxygen and almost zero order in ethylene with an apparent activation energy of 16 kcal/mol, in agreement with previous work by Cant and Hall (*4*). Turnover numbers obtained from Eq. (7) and the estimated catalyst surface area are within a factor of 2 or 3 from the reported turnover numbers of these authors at temperatures below 200°C under their "standard" conditions, i.e., P_{ET} = 20 Torr, P_{O_2} = 65 Torr.

The additional information obtained from the SEP measurements gives some new insight into the reaction mechanism.

That $a_0^2 < P_{O_2}$ shows that thermodynamic equilibrium is not established between surface and gas-phase oxygen during reaction. This implies that the intrinsic rate of oxygen adsorption is comparable with the intrinsic rate of the oxidation step. Furthermore Eq. (7) shows that the rate of oxygen adsorption is proportional to P_{O_2} and that one adsorbed oxygen atom reacts with one ethylene molecule in the rate-limiting step of the oxidation sequence. All this very strongly suggests the following slightly modified Carberry mechanism:

$$O_2(g) + m \underset{K_{-1}}{\overset{K_1}{\rightleftharpoons}} m \cdot O_2, \qquad (8)$$

$$m \cdot O_2 + m \underset{K_{-3}}{\overset{K_3}{\rightleftharpoons}} 2\,m \cdot O, \qquad (9)$$

$$2\{CH_2{=}CH_2 + m \cdot O \xrightarrow{K_2} m + P\}, \qquad (10)$$

where m stands for a surface site and P is a highly reactive intermediate which rapidly reacts with gas-phase oxygen to form CO_2 and H_2O.

On the basis of this model one can explain the steady-state kinetics as well as the steady-state surface oxygen activity behavior in a quantitative manner.

The dissociative oxygen adsorption is represented by steps (8) and (9). Oxygen adsorption is assumed to proceed via a molecularly adsorbed precursor state, in agreement with recent studies of O_2 adsorption on clean Pt surface (*21*). We assume that step (8) is rate limiting for O_2 adsorp-

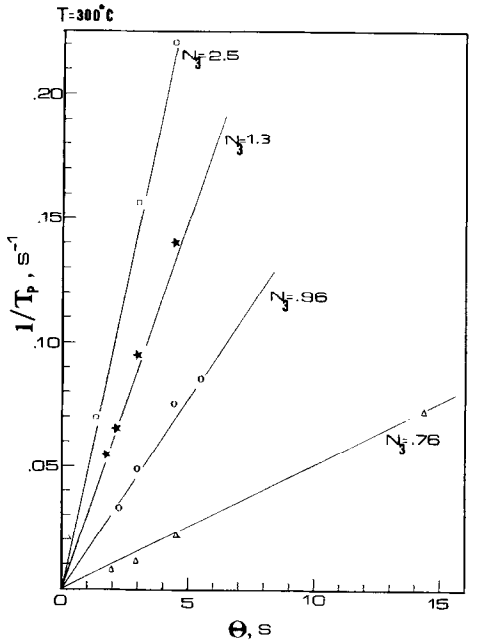

FIG. 14. Limit-cycle frequency vs residence time at T = 300°C.

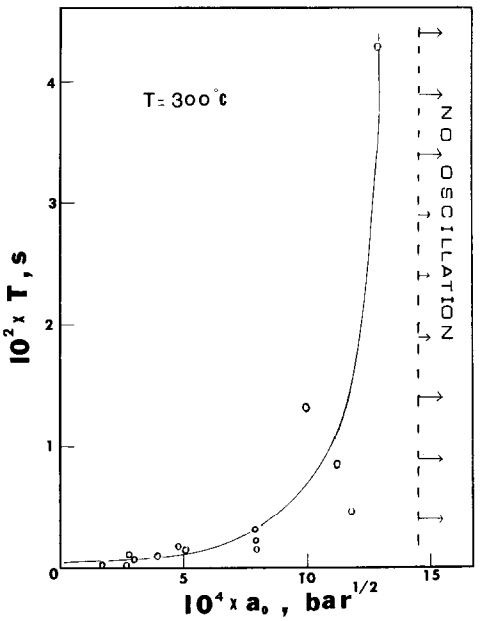

FIG. 15. Limit-cycle period vs average surface oxygen activity at 300°C.

tion and that step (9) is always in equilibrium. It then follows that the net steady-state rate of O_2 adsorption r_1 is given by

$$2r_1 = K_1 P_{O_2} \theta_m - K_{-1} \theta_{O_2} \qquad (11)$$

and that

$$\theta_{O_2} = K_{-3} \theta_O^2 / K_3 \theta_m, \qquad (12)$$

where θ_m is the fraction of free m-type surface sites and θ_O and θ_{O_2} are the coverages of atomically and molecularly chemisorbed oxygen, respectively, so that

$$\theta_m + \theta_O + \theta_{O_2} = 1. \qquad (13)$$

Molecularly chemisorbed oxygen $m \cdot O_2$ exists only in trace surface concentrations at temperatures of catalytic interest (*21*); therefore one may safely assume $K_{-3}/K_3 \ll 1$ or $\theta_{O_2} \ll 1$, which implies $\theta_m \approx 1 - \theta_O$ and according to (11) and (12):

$$2r_1 = K_1 P_{O_2}(1 - \theta_O) - K_{-1} \frac{K_{-3}}{K_3} \cdot \frac{\theta_O^2}{1 - \theta_O}. \qquad (14)$$

When equilibrium is established between surface oxygen and gas-phase oxygen, i.e., $P_{O_2} = a_O^2$ or $r_1 = 0$, Eq. (14) reduces to a Langmuir-type adsorption isotherm:

$$K_O^2 P_{O_2} = \theta_O^2/(1 - \theta_O)^2 \qquad (15)$$

with $K_O^2 = K_1 K_3 / K_{-1} K_{-3}$. According to Eq. (15) and the definition of the surface oxygen activity a_O^2 (Eq. 4), it follows that

$$K_O a_O = \theta_O/(1 - \theta_O). \qquad (16)$$

Note that this expression relates two intrinsic surface properties and is valid whether or not equilibrium with the gas phase exists. It is therefore valid under reaction conditions to the extent that ethylene does not compete with oxygen for the m sites.

The reaction between adsorbed atomic oxygen and gaseous ethylene is represented by step (10). The rate of this reaction is taken to be

$$r_2 = K_2 P_{ET} \theta_O. \qquad (17)$$

A steady-state mass balance on adsorbed atomic oxygen gives

$$O = 2r_1 - r_2 = K_1 P_{O_2}(1 - \theta_O) - K_{-1} \frac{K_{-3}}{K_3} \cdot \frac{\theta_O^2}{1 - \theta_O} - K_2 P_{ET} \theta_O. \qquad (18)$$

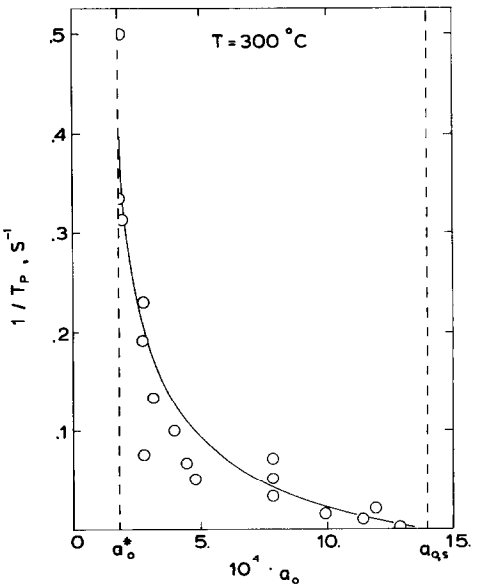

FIG. 16. Limit-cycle frequency vs average surface oxygen activity at 300°C.

Substituting Eq. (16) and simplifying:

$$P_{O_2} - a_0^2 = \frac{K_2}{K_1} P_{ET} \frac{\theta_O}{1 - \theta_O}. \quad (19)$$

Taking into account the experimental observation $P_{O_2} \gg a_0^2$, which is equivalent to assuming that oxygen desorption is slow compared to the oxidation reaction, one obtains

$$P_{O_2} = \frac{K_2}{K_1} \cdot P_{ET} \frac{\theta_O}{1 - \theta_O}, \quad (20)$$

which according to Eq. (16) is the experimental equation

$$a_0 = K_s P_{O_2}/P_{ET} \quad (6)$$

provided $K_s = K_1/K_2K_0$. It also follows from Eq. (20) that

$$\theta_O = K_1P_{O_2}/(K_1P_{O_2} + K_2P_{ET}) \quad (21)$$

and substituting into Eq. (17)

$$r = K_1K_2P_{ET}P_{O_2}/(K_1P_{O_2} + K_2P_{ET}),$$

which is the experimental rate expression (Eq. (7)).

Rate and Oxygen Activity Oscillations

Although the above model can explain the steady-state behavior in a quantitative way, it can be shown (*13*) that it does not predict the observed rate and surface oxygen activity limit-cycle behavior. It always predicts one stable steady state in a CSTR.

The origin of the limit cycles can be understood from the observation that limit cycles appear only with the surface oxygen activity a_0 exceeding a critical value $a_0^*(T)$. This observation very strongly suggests that a_0^* corresponds to the minimum surface oxygen activity necessary for the existence of a surface platinum oxide. This surface oxide does not form on m-type sites. When $a_0 > a_0^*$ the surface platinum oxide is stable. However, the oxide becomes unstable when the P_{ET}/P_{O_2} ratio in the reactor exceeds a critical value such that (Eq. (6)) $a_0 < a_0^*$. When this happens a significant amount of oxygen, previously associated with platinum oxide, becomes available for reaction at the catalyst surface. If one postulates that this "stored" oxygen can react rapidly with gaseous ethylene, then it becomes possible (*13*) to explain not only the appearance of limit cycles, but also the experimentally observed features of the oscillations in a CSTR, i.e., that

(i) Limit cycles appear on the fuel-rich side only, i.e., when $a_0 < 3K_s$.

(ii) The frequency is linear in N_3 and residence time.

(iii) The limit cycles occur between an upper and a lower temperature limit.

Qualitatively, a limit cycle can be described as follows. Immediately after ethylene has reacted with oxygen previously associated with the oxide, the ratio P_{ET}/P_{O_2} in the CSTR drops below the critical value corresponding to platinum oxide stability. Thus oxide formation becomes thermodynamically possible and takes place until the P_{ET}/P_{O_2} ratio increases to the critical value. At this point the oxide becomes unstable and rapidly reacts with ethylene, thus causing a spike in the rate of CO_2 formation while the P_{ET}/P_{O_2} ratio drops again below the critical value.

The existence of at least two different forms of oxygen sorbed on platinum has been established by TPD studies (*14*). Ostermaier *et al.* (*15*) have shown that one form corresponds to chemisorbed oxygen, the other to surface platinum oxide. The oxide is less reactive than chemisorbed oxygen and is unstable in reducing atmospheres. Oxide formation introduces a variability into the surface properties of platinum that makes reproducing catalytic activity difficult (*15*) and allows for an oxygen "storage" on platinum catalysts. This oxygen storage may be related to the observed oscillatory behavior of other catalytic oxidations on platinum (*16–19*).

Oscillations in the emf of solid-state oxygen concentration cells used in nonequilibrium CO, O_2 environments have already been reported and attributed to periodic variations of the surface oxygen

coverage of the Pt electrode (*20*). That rate oscillations were not previously reported for the ethylene oxidation on Pt must be due to the different temperature ranges employed in previous studies. Indeed the observed rate and oxygen activity oscillations occur over a rather narrow temperature range, roughly between 240 and 360°C.

The observation that oscillations take place only when the surface oxygen activity drops below a critical value corresponding to the stability limit of surface platinum oxide shows the usefulness of solid electrolyte potentiometry as a tool for the study of catalytic oxidations on metals.

ACKNOWLEDGMENTS

This research was supported under NSF Grant ENG 77-27500. Acknowledgment is also made to the Donors of the Petroleum Research Fund for partial support of this research under Grant 9893-G3.

REFERENCES

1. Dixon, J. K., and Longfield, J. E., *in* "Catalysis" (P. H. Emmett, Ed.), Vol. 7, p. 183. Reinhold, New York, 1960.
2. Margolis, L. Y., *Advan. Catal.* **14,** 429 (1963).
3. Voge, H. H., and Adams, C. R., *Advan. Catal.* **17,** 151 (1969).
4. Cant, N. W., and Hall, W. K., *J. Catal.* **16,** 220 (1970).
5. Carberry, J. J., *Kinet. Katal.* **18**(3), 562 (1977).
6. Wagner, C., *Advan. Catal.* **21,** 323 (1970).
7. Vayenas, C., and Saltsburg, H., *J. Colloid Interface Sci.* **3,** 261 (1976).
8. Vayenas, C., and Saltsburg, H., *J. Catal.* **57,** 296 (1979).
9. Stoukides, M., and Vayenas, C., *J. Catal.* **64,** 18 (1980).
10. Dietz, H., Haecker, W., and Jahnke, H., *in* "Advances in Electrochemistry and Electrochemical Engineering" (H. Gerischer and C. W. Tobias, Eds.), Vol. 10, p. 1. Wiley–Interscience, New York, 1977.
11. Kleitz, M., Fabry, P., and Schoule, E., *in* "Electrode Processes in Solid State Ionics" (M. Kleitz and J. Dupuy, Eds.). Reidel, Dordrecht, 1976.
12. Weinberg, W. H., and Merrill, R. P., *Surface Sci.* **39,** 206 (1973).
13. Vayenas, C., Georgakis, C., and Michaels, J., *J. Catal.*, in press.
14. Procop, M., and Völter, J., *Z. Phys. Chem. (Leipzig)* **250,** 387 (1972).
15. Ostermaier, J., Katzer, J., and Manogue, W., *J. Catal.* **41,** 277 (1976).
16. Sheintuch, M., and Schmitz, R., *in* "5th International Symposium on Chemical Reaction Engineering," *ACS Symp. Ser.* **65,** 487 (1978).
17. Varghese, P., Carberry, J., and Wolf, E., *J. Catal.* **55,** 76 (1978).
18. Dauchot, J., and Van Cakenberghe, J., *Nature Phys. Sci.* **246,** 61 (1973).
19. Cutlip, M., and Kenney, C., *in* "5th International Symposium on Chemical Reaction Engineering," *ACS Symp. Ser.* **65,** 475 (1978).
20. Hetrick, R., and Logothetis, E., *Appl. Phys. Lett.* **34**(1), 117 (1979).
21. Gland, J. L., and Korchak, V. N., *Surface Sci.* **75,** 733 (1978).
22. Lee, B., S. M. Thesis, Massachusetts Institute of Technology (1980).
23. Stoukides, M., and Vayenas, C. G., submitted for publication.